

# Three-dimensional image encryption, transmission and processing by using digital holography

Bahram Javidi<sup>1</sup>, Enrique Tajahuercé<sup>2</sup>, Thomas J. Naughton<sup>3</sup>, Yann Frauel<sup>4</sup>, and Osamu Matoba<sup>5</sup>

<sup>1</sup> Electrical and Computer Engineering Department, University of Connecticut, Storrs, CT 06269-2157, USA.

<sup>2</sup> Departament de Ciències Experimentals, Universitat Jaume I, 12080 Castellón, Spain.

<sup>3</sup> Department of Computer Science, National University of Ireland/Maynooth, Maynooth, County Kildare, Ireland.

<sup>4</sup> IIMAS, Universidad Nacional Autónoma de México, 01000 México, D.F., México.

<sup>5</sup> Department of Computer and Systems Engineering, Kobe University, Kobe 657-8501, Japan.

## ABSTRACT

We describe several methods for optoelectronic processing of 3D images based in digital holography. In all cases, phase-shift digital holography is used to record the complex amplitude distribution associated to the diffraction field generated by 3D objects illuminated with coherent light. First, we review a technique to encrypt a 3D image by using digital holography. Encryption is performed by using random phase codes as key functions. In this way, it is possible to send secure 3D information through conventional digital communication lines. In our approach, decryption is carried out digitally. Next we describe both, digital and optical reconstruction of 3D images starting from digital holograms. Finally, we show how to perform 3D pattern recognition with high discrimination based in the above techniques. Experimental results are presented.

**Keywords:** Optical security and encryption, digital holography, 3D image processing, 3D patter recognition.

## 1. INTRODUCTION

Application of optical processing systems to security, verification, and encryption of information has proved to be a real alternative to electronic processing.<sup>1-6</sup> The information to be secured or verified is optically processed after being encoded as a two-dimensional image by using amplitude, phase, polarization or wavelength modulation of light. In one approach, random phase-codes can be used to encrypt the information by modifying the Fraunhofer or Fresnel diffraction patterns of the input image,<sup>2,3,6</sup> as in methods for securing or multiplexing holographic memories.<sup>7-12</sup> However, the encrypted image contains both amplitude and phase and thus holographic recording is required, which makes difficult to transmit the encrypted information over conventional communication channels.

Several digital holography methods have been applied to record fully complex information with electronic cameras.<sup>13-15</sup> Among them, digital phase-shifting interferometry stands out as a versatile and efficient technique.<sup>16-18</sup> In this direction, encryption of 2D images has already been reported by using off-axis and in-line digital holography.<sup>19,20</sup> Advantages of optical encryption as speed, large number of degrees of freedom and high security, are combined with the usefulness of electronic information transmission.

In addition to the previous advantages, digital holography techniques are well adapted to process 3D information, and this fact allows us to develop optical security techniques able to process 3D images. In this work we review several of these methods. In all the cases, phase-shift digital holography is used to record the complex amplitude distribution of the diffraction patterns generated by 3D objects illuminated with coherent light. As an approach to these techniques, first we describe an optical encryption procedure that uses phase-shifting interferometry to record the fully-complex encrypted information of a 2D image.<sup>20</sup>

Next, we apply the previous idea to optically secure 3D information.<sup>21</sup> In this approach, a phase-shifting interferometer records the phase and amplitude information generated by a 3D object at a plane located in the Fresnel diffraction region by using an intensity recording device. This information is encrypted optically with the Fresnel diffraction pattern generated by a random phase mask and stored electronically. The key is also electronically recorded by phase-shifting interferometry. The decrypted image can be obtained digital or optically by using the complex field associated to the key.

We also describe a method to reconstruct the 3D object optically by using only the phase information of a digital hologram.<sup>22</sup> The proposed method is suitable for real-time optical reconstruction of the 3D object and takes advantage of minimal optical power loss in the reconstruction process.

Finally, we show a method for recognition of 3D objects by using digital holography. Holographic methods are attractive to perform 3D image recognition since a single hologram is able to record 3D information of the object, avoiding sequential recording of several 2D perspectives and maintaining the phase information. In our approach, pattern recognition using 3D information can be performed by applying correlation techniques to the information contained in the digital holograms<sup>23</sup>.

We would like to point out that other optoelectronic 3D image processing operations based in the above methods are also possible. In particular, our pattern recognition method has been extended to achieve shift invariance along the optical axis.<sup>24</sup> Furthermore, we have used nonlinear composite correlation filters to achieve distortion tolerance.<sup>25</sup> To improve the method, we have developed a two-layer neural network for processing of 3D images that are obtained by digital holography.<sup>26</sup> In a recent paper, we have compared passive ranging integral imaging and active imaging digital holography for 3D object recognition.<sup>27</sup> Moreover, we have applied compression techniques to digital holograms for the efficient transmission of 3D images.<sup>28,29</sup>

The contribution is structured in the following way. Section 2 describes how digital phase-shifting interferometry can be adapted to encrypt the Fresnel diffraction pattern of a 2D input. In Section 3 we show how to extend this technique to the encryption of 3D scenes. In Section 4 we describe the optical reconstruction of a digital hologram. In Section 4 we outline an approach to perform 3D image recognition with digital holography, and a technique to measure 3D orientation changes. Finally, Section 5 summarizes the conclusions.

## 2. ENCRYPTION OF 2D IMAGES WITH DIGITAL HOLOGRAPHY

The first optical encryption system described in this work is depicted in Fig. 1.<sup>20</sup> It is based on a Mach-Zehnder interferometer. An Argon laser beam, expanded and collimated, is divided by a beam splitter into two plane wave fronts traveling in different directions. After reflecting in a mirror, the object beam impinges on the input transparency whose amplitude transmittance,  $t_O(x,y)$ , contains the data to be encrypted. The light diffracted by the input object impinges into the CCD detector through the second beamsplitter. By measuring the complex amplitude distribution of the Fresnel diffraction pattern at the output plane,  $U_H(x,y)$ , the amplitude of the input function,  $t_O(x,y)$ , may be recovered computing an inverse Fresnel transform operation either optically or numerically.

The parallel reference beam passes through two phase retarders, one quarter and one half wave plate, is reflected by a mirror, and is modified by a second random phase mask. The system is aligned in such a way that, without the phase mask, the reference beam generates a plane wave traveling perpendicular to the CCD sensor after reflecting in the second beam splitter. The light provided by the Argon laser is linearly polarized. In this way, by suitably orienting the phase retarders, the phase of the reference beam can be shifted to different values. Let us assume that the phase of the parallel beam after the second retarder plate is  $\varphi_0$  when the fast axis of both plates is aligned with the direction of polarization. In this way, by aligning successively the different slow and fast axes of the phase retarders with the direction of polarization of the incident light, different phase values  $\varphi_0 + \alpha_p$  with  $\alpha_1=0$ ,  $\alpha_2=-\pi/2$ ,  $\alpha_3=-\pi$ , and  $\alpha_4=-3\pi/2$  can be produced.

The reference phase mask has a random phase distribution  $\phi_R(x,y)$  and is placed at a distance  $L=L_1+L_2$  from the CCD detector, as shown in Fig. 1. The complex amplitude distribution of the reference beam at the output plane can be denoted by  $U_R(x,y;\alpha_p)$ , where  $\alpha_p$  denotes the relative phase changes introduced by the retarder plates on the reference beam. Other constant phase factors have been omitted in the previous equation.

The complex light field at the output plane can be evaluated with digital phase-shifting interferometry by recording four intensity patterns with the reference beam phase shifted by the previous values of  $\alpha$ .<sup>19</sup> Denoting the complex amplitude distribution at the output plane generated by the object and the reference beams with

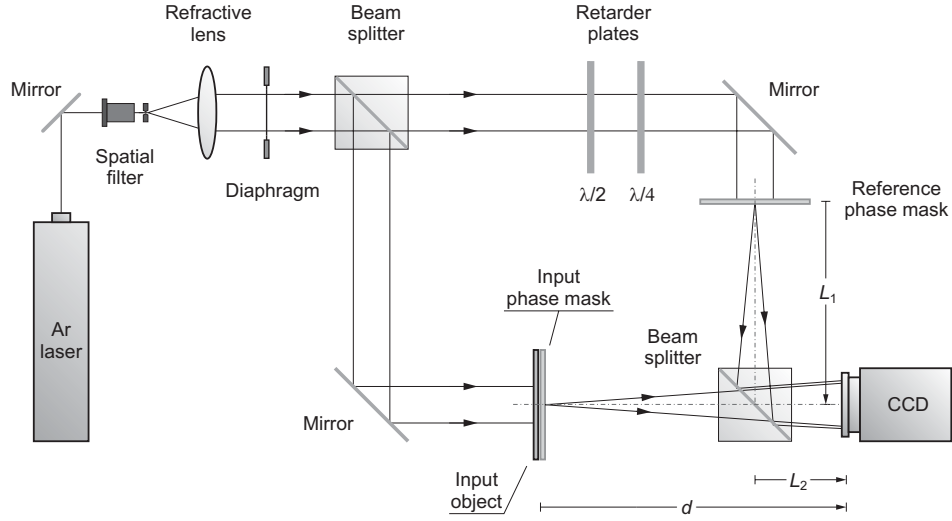


Figure 1. Phase-shifting interferometer for optical encryption of 2D objects.

$U_H(x,y)=A_H(x,y)\exp[i\phi_H(x,y)]$  and  $U_R(x,y;\alpha_p)=A_R(x,y)\exp[i(\phi_R(x,y)+\alpha_p)]$ , respectively, intensity pattern recorded by the linear intensity recording device is given by

$$I_p(x,y)=[A_H(x,y)]^2+[A_R(x,y)]^2+2A_H(x,y)A_R(x,y)\cos[\phi_H(x,y)-\phi_R(x,y)-\alpha_p] \quad (1)$$

It is straightforward to show that this phase-shifting interferometry technique provides the following encrypted phase

$$\phi_E(x,y)=\phi_H(x,y)-\phi_R(x,y)=\arctan\left[\frac{I_4(x,y)-I_2(x,y)}{I_1(x,y)-I_3(x,y)}\right] \quad (2)$$

The amplitude of the encrypted image is just the product of the amplitudes

$$A_E(x,y)=A_H(x,y)A_R(x,y)=\frac{1}{4}\left\{[I_1(x,y)-I_3(x,y)]^2+[I_4(x,y)-I_2(x,y)]^2\right\}^{1/2} \quad (3)$$

Note that it is not possible to recover the complex amplitude distribution  $U_H(x,y)$  generated by the object beam without knowledge of the random-like functions  $\phi_R(x,y)$  and  $A_R(x,y)$ . The input information is encrypted such that it can only be decrypted with the reference complex amplitude distribution  $U_R(x,y;0)$  or using the same reference phase mask  $\phi_R(x,y)$  located in the proper 3D position, which is acting as the key. In order to decrypt the information obtaining the original complex amplitude distribution  $U_H(x,y)$  we use again the phase-shifting interferometry technique to achieve the key complex distribution  $U_R(x,y;0)$ . By simply removing the input transparency in the optical system in Fig. 1, the phase and the amplitude of the Fresnel diffraction pattern generated by the reference random phase mask can be measured. The phase,  $\phi_K(x,y)$ , and amplitude,  $A_K(x,y)$ , provided by the phase-shifting interferometric technique are now

$$\phi_K(x,y)=\phi_C-\phi_R(x,y)=\arctan\left[\frac{I'_4(x,y)-I'_2(x,y)}{I'_1(x,y)-I'_3(x,y)}\right] \quad (4)$$

and

$$A_K(x, y) = A_C A_R(x, y) = \frac{1}{4} \left\{ [I'_1(x, y) - I'_3(x, y)]^2 + [I'_4(x, y) - I'_2(x, y)]^2 \right\}^{1/2}, \quad (5)$$

where  $I'_p(x, y)$  are the new interferograms obtained with the four different phase shifts  $\alpha_p$ . Parameters  $\phi_C$  and  $A_C$  in the previous equations are the constant amplitude and phase of the object beam at the output plane and can be simply substituted by 0 and 1, respectively. Thus Eqs. (4) and (5) allow to obtain directly the phase  $\phi_R(x, y)$  and amplitude  $A_R(x, y)$ . The decrypted complex amplitude distribution,  $U_D(x, y)$ , can be obtained combining Eqs.(6) and (7) with Eqs.(4) and (5) to obtain the phase

$$\phi_D(x, y) = \arctan \left[ \frac{(I_4 - I_2)(I'_1 - I'_3) - (I_1 - I_3)(I'_4 - I'_2)}{(I_4 - I_2)(I'_4 - I'_2) - (I_1 - I_3)(I'_1 - I'_3)} \right], \quad (6)$$

and the amplitude

$$A_D(x, y) = \left[ \frac{(I_1 - I_3)^2 + (I_4 - I_2)^2}{(I'_1 - I'_3)^2 + (I'_4 - I'_2)^2} \right]^{1/2}. \quad (7)$$

for simplicity, in Eqs. (8) and (9) the spatial dependence of  $I_p(x, y)$  and  $I'_p(x, y)$  has been omitted. This phase and amplitude functions reproduce the phase and amplitude of the diffraction pattern  $U_H(x, y)$ . Therefore by proper propagation of  $U_D(x, y)$ , using the Fresnel-Kirchhoff integral, it is possible to obtain the amplitude distribution in any other plane of the incident light beam within the paraxial approximation. Reconstruction can be implemented both optically, by encoding the complex distribution  $U_D(x, y)$  as a computer generated hologram, or digitally.

For direct computer reconstruction the following inverse discrete Fresnel transformation is performed,

$$|t(m', n')|^2 = \left| \sum_{m=0}^{N-1} \sum_{n=0}^{N-1} U_D(m, n) \times \exp \left[ -i\pi \frac{\Delta x^2}{\lambda d} (m^2 + n^2) \right] \exp \left[ i \frac{2\pi}{N} (mm' + nn') \right] \right|^2, \quad (8)$$

where  $m$  and  $n$  are the discrete spatial coordinates in the CCD plane and  $m', n'$  are the corresponding to the object plane. If we consider only the horizontal transversal direction, we have  $x = m\Delta x$  and  $x' = m'\Delta x'$ , being  $\Delta x$  and  $\Delta x'$  the spatial resolutions in the CCD plane and the input plane respectively. In Eq. (8) it is assumed that the number of pixels in both orthogonal directions of the CCD is the same, denoted by  $N$ . Eq. (8) can be calculated through a fast Fourier transform algorithm (FFT).<sup>30</sup> The resolution in the input plane is given by

$$\Delta x' = \frac{\lambda d}{N\Delta x} = \frac{\lambda d}{T}, \quad (9)$$

where  $T$  is the transversal size of the CCD.

The optical system in Fig.1 was experimentally constructed using an Argon laser emitting a vertical polarized light beam with  $\lambda = 514.5$  nm. The retarder plates were  $\lambda/2$  and  $\lambda/4$  wave plates optimized for the preceding wavelength. The four-step phase shifting was performed by rotating the phase retarders. The input image, with the input phase mask bonded, was located at a distance  $f$  from L. The input information was encoded as a binary image in a black and white transparency. The reference phase mask was located in the reference beam of the interferometer at a distance  $L = 300$  mm from the CCD. The different interferograms were registered by a CCD camera, sampled with  $480 \times 480$  pixels, and quantized to 8 bits of gray levels using a frame-grabber.

Figure 2 shows a gray level picture of the computer reconstructed image of the input to be encrypted. It was obtained recording a Fresnel diffraction pattern by phase-shifting interferometry without the reference phase mask. Once the phase and amplitude at the CCD plane were obtained, an inverse Fresnel transform algorithm was applied to recover the input image in the computer. The encrypted phase and amplitude distributions after locating the reference phase mask as indicated in Fig. 1 are shown in Figs. 3(a) and (b), respectively, as grey level pictures. By inverse Fresnel transformation of the complex amplitude distribution associated to these images we obtain the picture in Fig. 3(c). Note that only a random-like intensity pattern is obtained.



Figure 2. Image of the input object for Fresnel encryption obtained with a lensless phase-shift interferometer without reference phase mask.

In order to decrypt the previous information the key phase and amplitude functions were measured using Eqs.(6) and (7). These distributions are shown in Fig.4(a) and (b) as grey level pictures. By correcting the images in Fig. 4(a) and (b) with the proper decryption key, as it is stated in Eqs.(8) and (9) it is possible to reconstruct the original input image by an inverse Fresnel transformation in the computer. The decrypted image, almost identical to the original one, is shown in Fig. 4(c). The experimental results prove the feasibility of this technique.

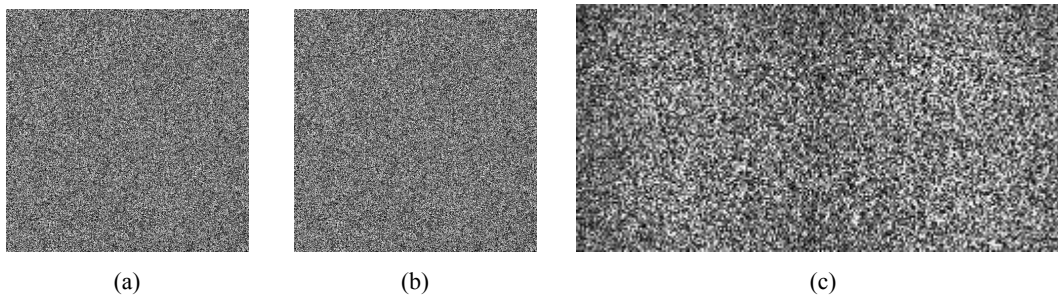


Figure 3. Result of the 2D encryption experiment with Fresnel encryption: (a) and (b) are grey level pictures of the encrypted phase and amplitude of the input object. (c) is an attempt of direct reconstruction from the encrypted hologram.

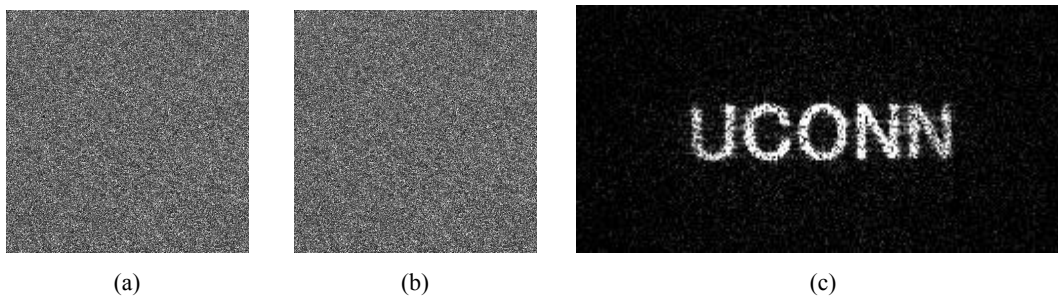


Figure 4. Result of the 2D decryption experiment: (a) and (b) are grey level pictures of the phase and amplitude of the key. (c) shows the decrypted image when the encrypted hologram is corrected with the proper key.

### 3. ENCRYPTION OF 3D INFORMATION

The ideas described in the previous section have been also applied to secure information codified in a 3D scene.<sup>21</sup> The method is based in the ability of digital holograms to reconstruct in the computer images of 3D objects focused at different planes. Encryption is performed by recording the interference of a Fresnel diffraction pattern of the 3D input with a Fresnel pattern generated by a random phase mask. Decryption in the computer is only possible with information about the reference phase mask. Furthermore, it has been shown that, after decryption, not only different focusing planes but also different perspectives of the 3D input can be obtained by properly modifications of the digital Fresnel hologram.

The outline of the optical system to encrypt 3D information is shown in Fig. 5. It is also based on a Mach-Zehnder interferometer architecture. Collimated light from the Argon laser is divided by beam splitter BS<sub>1</sub> into the reference and the object beams. With diaphragm D<sub>2</sub> open, the object beam illuminates the 3D input. Assuming that the incident light is diffracted only once, we can describe the opaque object as a 3D continuum distribution of point sources with relative amplitude  $U_O(x,y,z)$ , where  $x$ , and  $y$  are transversal coordinates and  $z$  is the paraxial distance to the output plane. This object generates a complex amplitude distribution  $U_H(x,y)$  at the output plane that can be evaluated with a 3D integral of superposition

The parallel reference beam travels through the retarder plates and is diffracted by a random phase mask. The phase retarders are again a quarter,  $\lambda/4$ , and a half,  $\lambda/2$ , wave plates. They modulate the phase of the reference beam with four phase shifts values  $\alpha_p$  by aligning the fast and slow axes of the retarders. The phase mask, with a random phase distribution  $\Phi_R(x,y)$ , is located at an arbitrary distance  $L=L_1+L_2$  from the detector, and generates a complex field  $U_R(x,y;\alpha_p)$ .

The output intensity results from the coherent superposition of the diffraction patterns  $U_H(x,y)$  and  $U_R(x,y;\alpha_p)$ , and can be written as in Eqs. (1), where now functions  $A_H(x,y)$ , and  $\phi_H(x,y)$  are the amplitude and phase distribution generated by the 3D object at the output plane. Recording four interference patterns  $I_p(x,y)$  with the reference phase shifted by the four values  $\alpha_p$ , it is straightforward to show that the measured phase is given by Eqs. (2) and (3).

The amplitude  $A_E(x,y)$  and phase  $\phi_E(x,y)$  constitute the encrypted hologram. Without knowledge of the functions  $A_R(x,y)$  and  $\phi_R(x,y)$ , which act as keys for the decryption, it is not possible to recover images of the 3D object by inverse Fresnel propagation. To obtain the key functions, diaphragm D<sub>3</sub> is open and the object is removed. The reference and object parallel beams impinge in-line into the output plane. In this way, we record other four intensity patterns  $I'_p(x,y)$

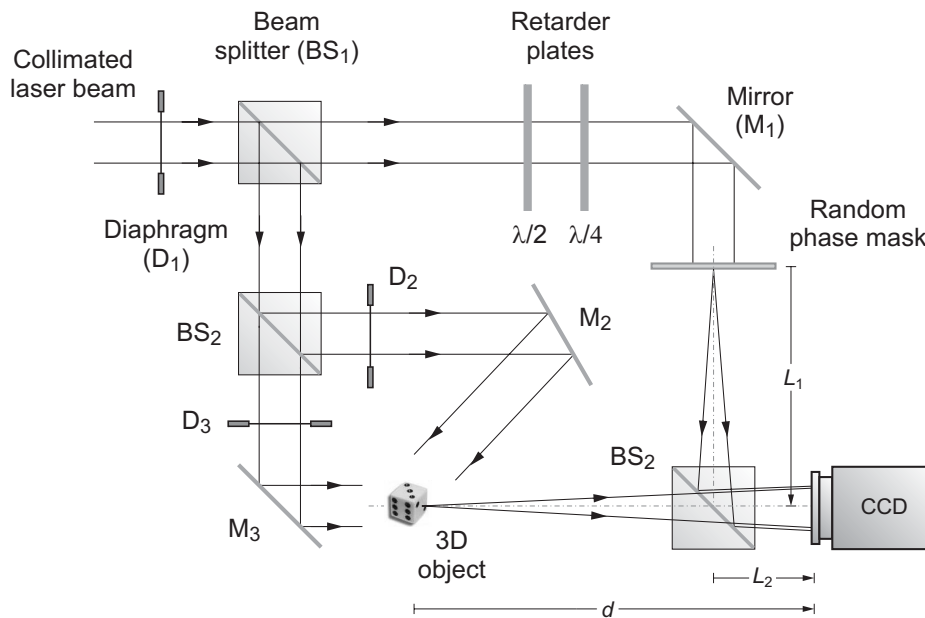


Figure 5. Phase-shifting interferometer for optical encryption of 3D objects.

that, by applying Eqs.(4) and (5), provide the phase  $\phi_K(x,y)=\phi_C-\phi_R(x,y)$  and the amplitude  $A_K(x,y)=A_C A_R(x,y)$  generated by the phase mask. As in the previous Section, parameters  $\phi_C$  and  $A_C$  are the constant phase and amplitude of the object beam and can be substituted by 0 and 1, respectively. Decryption is performed by combining the encrypted hologram, determined by  $A_E(x,y)$  and  $\phi_E(x,y)$ , with the key functions  $A_K(x,y)$  and  $\phi_K(x,y)$  using the expressions in Eqs. (6) and (7). Decrypted functions,  $A_D(x,y)$  and  $\phi_D(x,y)$ , constitute now the amplitude and phase of the decrypted Fresnel digital hologram,  $U_D(x,y)$ , of the 3D object. By free-space propagation of  $U_D(x,y)$  the amplitude distribution of the input object can be reconstructed.

Digital reconstruction of the input object  $U_O(m',n')$  can be performed by computing a Fresnel integral similar to that in Eq. (8) numerically, being now  $U_D(m,n)$  the discrete amplitude distribution of the decrypted digital hologram of the 3D object. Note that different regions of the hologram record light arising from different perspectives of the 3D object. Thus, we can reconstruct different views of the 3D object by using different windows in the decrypted hologram and illuminating them with tilted plane waves. Points on the surface of the object at distances  $z$  from the hologram different than  $d$  will appear defocused in the reconstructed image. Nevertheless, the location of the planes of reconstruction can also be changed easily in the computer starting from the same digital hologram. Note also that the field of focus can be increased diminishing the size of the hologram window at the expense of a reduction of resolution.

Encryption of a 3D object was performed experimentally with the phase-shift interferometer architecture depicted in Fig. 5. In Fig. 6 we show the axial view of the object generated from a non encrypted digital hologram using Eq. (8).

The entire digital hologram was used for the reconstruction. The 3D object to be encrypted was located at a distance  $d=570$  mm from the CCD. Figs. 7(a) and (b) show grey level pictures of the amplitude and phase distributions of the encrypted hologram when the random phase mask is located as shown in Fig. 5. The amplitude and phase distributions generated by the random phase mask at the output plane were also measured by removing the object and opening diaphragm  $D_3$ . From the previous encrypted and key intensity patterns the decrypted hologram was obtained by using Eqs. (8) and (9). The decrypted image shown in Fig. 7(c) was generated using the entire decrypted hologram. For comparison, in Fig. 7(d) we show a decryption performed without the correct key. Only a random-like pattern is obtained.



Figure 6. Image of the original 3D object to be encrypted obtained by phase-shift interferometry with the optical system in Fig. 5 without reference phase mask.

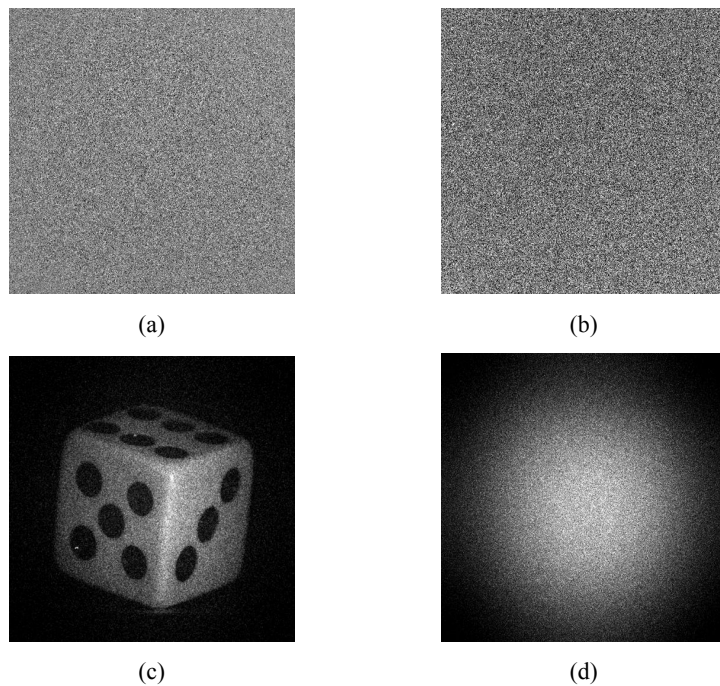


Figure 7. Result of the encryption experiment: Encrypted amplitude and phase in (a) and (b), respectively; decrypted image in (c); and incorrect decryption in (d).

#### 4. OPTICAL RECONSTRUCTION OF DIGITAL HOLOGRAMS

In this section, we describe an optical reconstruction method to display 3D objects from digital holograms.<sup>22</sup> The reconstruction is performed by use of phase-only information of the optical complex field. In this way, the phase-only reconstruction enables us to use commercially available displays such as liquid crystal spatial light modulators (SLM).

First, we show that it is possible to reconstruct a 3D object from phase-only information of the digital hologram as well as from the whole complex-field. The experimental setup to obtain the digital hologram, based in a four-step phase-

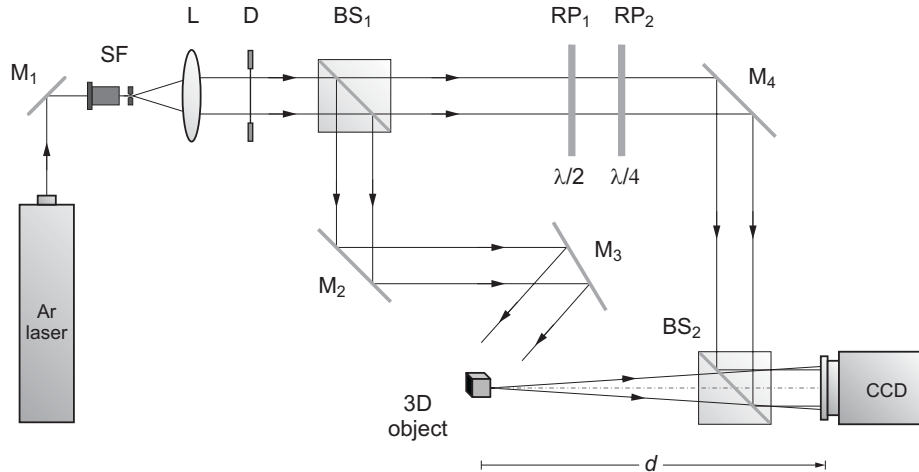


Figure 8. Optical system to record the digital hologram of a 3D object.

shift interferometer, is shown in Fig. 8. The object beam illuminates the input 3D object, and the reference beam forms an in-line interference pattern with the light diffracted by the object onto the CCD camera. In Fig. 8, L is a refractive lens, D is a diaphragm, SP denotes a spatial filter, BS<sub>1</sub> and BS<sub>2</sub> are beam splitters, M<sub>1</sub> to M<sub>4</sub> are plane mirrors, RP<sub>1</sub> and RP<sub>2</sub> are two wave retarder plates with retardation  $\lambda/2$  and  $\lambda/4$ , respectively, and  $\lambda$  is the wavelength of the light. Again, the four phase retardation 0,  $\pi/2$ ,  $\pi$ , and  $3\pi/2$  is implemented by the combination of directions of the half- and quarter-wave plates. The object is a 3D die with dimensions  $5 \times 5 \times 5$  mm and is located at a distance of 322 mm from the CCD.

Figures 9(a) and (b) show the numerically reconstructed 3D object using complex information and phase-only information, respectively. From the figure, we see that phase-only information can reconstruct the 3D object successfully but with speckle noise. To reduce speckle, we apply a low pass filter (mean filtering) to the reconstructed 3D object. The low-pass filtered images are presented in Figs. 9(c) and 9(d).

In practical systems, there is a limit on the number of phase levels that can be displayed in phase-only spatial light modulators (P-SLMs). Reconstructions from phase-only information are compared with intensity images reconstructed from fully complex information, for different

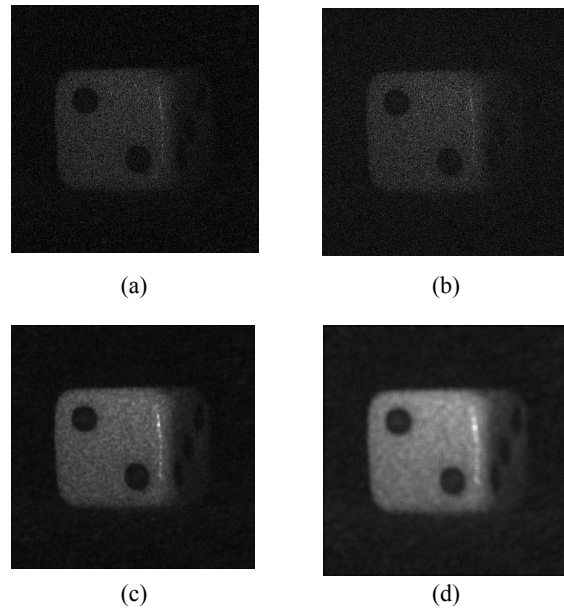


Figure 9 Numerically reconstructed 3D object from (a) complex field, (b) phase-only, (c) low-pass filtered with mean filter of  $11 \times 11$  pixels and (d)  $21 \times 21$  pixels after reconstruction using phase-only information.

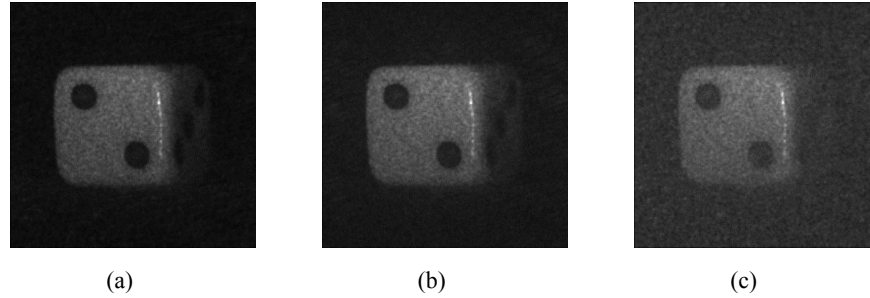


Figure 10. Reconstructed 3D object of the die without quantization reduction, and with quantization reductions to 4 bits and 1 bit.

numbers of quantization levels. For these calculations, we use a mean filter with  $11 \times 11$  pixels. Figure 10 shows the reconstructed 3D object without quantization reduction, and with quantization reductions to 4 bits and 1 bit. Note that we can discern the 3D object even when the phase level of the P-SLM is binary.

The optical setup to reconstruct 3D objects is shown in Fig. 11. After collimation and beam-width expansion, a He-Ne laser beam illuminates a liquid crystal SLM with  $1024 \times 768$  pixels. The size of each pixel is approximately  $18 \mu\text{m} \times 18 \mu\text{m}$ . The maximum amount of phase retardation possible with our SLM is  $0.6\pi$ . Figure 12 shows the reconstructed 3D die. Figures 8(a), (b) and (c) contain reconstructions with the CCD located at distances of 113 mm, 123 mm, and 133 mm from the SLM, respectively. From these figures, we can see that the object is reconstructed at different planes. The calculated positions of the in-focus reconstructions are 104 mm and 126 mm, respectively. These systematic errors are caused by our use of a different readout wavelength, different pixel size, and a readout wavefront not exactly the same as a plane wave.

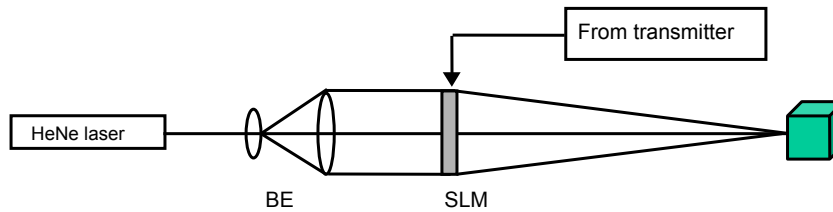


Figure 11. Optical reconstruction by use of phase-only information of digital hologram.

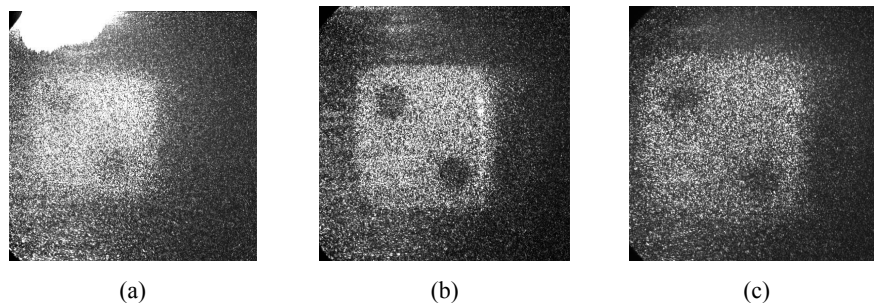


Figure 12. Experimental results; (a), (b) and (c) are reconstructed images of the die where the CCD is located at 113 mm, 123 mm, and 133 mm from the SLM, respectively.

#### 4. THREE-DIMENSIONAL PATTERN RECOGNITION BY DIGITAL HOLOGRAPHY

The ability of digital holograms to record a perspective of a 3D input object has been also applied to develop a versatile technique for 3D pattern recognition.<sup>23</sup> Utilizing phase-shifting interferometry, digital holograms of Fresnel diffraction patterns associated to the 3D input scene and a 3D reference pattern are recorded. In this way, different pattern recognition techniques based on the information contained in the digital holograms can be performed.

The first step of this optoelectronic procedure to perform 3D pattern recognition is to record a digital hologram of the 3D objects under study. The optical system for the digital holographic recording step is the same depicted in Fig. 8. The complex amplitude distribution due to the object beam at the CCD detector is denoted again as  $U_H(x,y)$ . The complex field generated by the reference at the output plane can be written as  $U_R(x,y;\alpha)=A_R \exp[i(\varphi+\alpha_p)]$  where  $\varphi$  is the constant phase when both fast axes of the retarder plates are aligned with the direction of polarization and  $\alpha_p$  is the phase shift in other configurations. As in the previous section, by aligning the slow and fast axes of the retarders, phase-shifts  $\alpha_1=0$ ,  $\alpha_2=\pi/2$ ,  $\alpha_3=\pi$ , and  $\alpha_4=3\pi/2$  are produced without altering the constant amplitude  $A_R$ . Note that other real time phase shifting techniques, using piezoelectric mirrors or liquid crystal displays, for example, can also be applied.

The amplitude distribution  $U_H(x,y)$  is measured by phase-shifting interferometry recording four intensity patterns  $I_p(x,y)=|U_H(x,y)+U_R(x,y;\alpha)|^2$ . By properly combining these interferometric patterns, following the same procedure described in the previous sections, we are able to measure the phase

$$\phi_D(x,y) = \phi_H(x,y) - \varphi_R \quad , \quad (10)$$

and the amplitude

$$A_D(x,y) = A_H(x,y)A_R \quad . \quad (11)$$

The phase  $\varphi_R$  and amplitude  $A_R$  of the reference beam are constant factors and can be substituted by 0 and 1, respectively. In this way, the recorded digital hologram  $U_D(x,y)=A_D(x,y)\exp[i\phi_D(x,y)]$  provides directly the complex field diffracted by the 3D object.

As in previous sections, the object amplitude distribution,  $U_O(m,n)$ , can be numerically evaluated with a single fast Fourier transform algorithm, as in Eq.(8). But an alternative way is to use the propagation transfer function method, which implies two fast Fourier transformations, i.e.,

$$U_O(m,n) = \mathcal{F}^{-1} \left\{ \mathcal{F} [U_D(m,n)] \times \exp \left[ -i\pi\lambda d \left( \frac{u^2}{(\Delta x' N_x)^2} + \frac{v^2}{(\Delta y' N_y)^2} \right) \right] \right\} \quad , \quad (12)$$

where  $\mathcal{F}$  denotes the discrete Fourier transformation, and  $u$  and  $v$  are discrete spatial frequencies.

To perform recognition of 3D objects we use a Fourier matched filter approach applied to the information obtained by digital holography. Let us consider a second 3D object,  $U_P(x,y,z)$ , located also at a distance  $d$  from the CCD, and its corresponding digital Fresnel hologram,  $U_G(x,y)$ . The correlation between a view of this 3D input object with a given perspective of the reference object  $U_O(x,y,z)$  can be evaluated from the hologram  $U_G(x,y)$  by digital reconstructing the object with Eq. (12) and computing the correlation between the reconstructed images. An alternative way to perform the operation of correlation more efficiently is described next. Using Eq. (12), the correlation intensity of the reference amplitude distribution  $U_O(m,n)$  with that of the input  $U_P(m,n)$  generated from the holograms, can be written as

$$\begin{aligned} C_{OP}(m,n) &= \left| \mathcal{F}^{-1} \left\{ \mathcal{F} \{U_O(m,n)\} \mathcal{F}^* \{U_P(m,n)\} \right\} \right|^2 = \\ &= \left| \mathcal{F}^{-1} \left\{ \mathcal{F} \{U_D(m,n)\} \mathcal{F}^* \{U_G(m,n)\} \right\} \right|^2 \quad . \end{aligned} \quad (13)$$

Thus, by performing the correlation between the two Fresnel digital holograms we are evaluating the correlation between perspectives of the 3D objects. Note that rough objects involve fast fluctuations of the reconstructed phase under translations, thus reducing the shift invariance.

We would like to note that, as in conventional analogue holography, different regions of the digital hologram record different perspectives of the 3D input object, which can be reconstructed by proper numerical propagation of the discrete distribution  $U_D(m,n)$ . The discrete complex amplitude distribution at different planes in the object beam subtending angles  $\alpha$  and  $\beta$  with the optical axis can be numerically computed, within the paraxial approximation and aside from constant factors, by using a discrete Fresnel transformation similar to that in Eq. (12). Now, to obtain different perspectives, this equation needs to be modified by extracting only a partial window from the digital hologram and by considering a linear phase factor to take into account the direction of observation.

Note also that by performing the correlation between different regions of the two holograms, properly modified by a linear phase factor, we achieve the correlation between different perspectives of the 3D objects. This allows to design measurement techniques with high sensitivity. This fact is illustrated by measuring a small rotation of a rough 3D object.

A 3D object recognition experiment was carried out using two reproductions of cars with an approximate size of  $25 \times 25 \times 45$  mm. They were located at a distance  $d=865$  mm from the CCD detector. The grey level pictures (a) and (b) in Fig. 13 were obtained by recording a digital hologram of each car model denoted by  $U_D(x,y)$  and  $U_G(x,y)$ , respectively. The reconstruction of the digital holograms was performed by computing a fast Fourier transform algorithm applied to the entire hologram.

In Fig. 14(a) we show a plot of the autocorrelation of the object in Fig. 13(a) performed by using a partial digital hologram obtained by placing a window centered at the origin of  $U_D(x,y)$ . Figure 14(b) shows the crosscorrelation of the 3D object in Fig. 13(a) with that in Fig. 13(b) obtained also by digital holography. The operation of correlation was performed with Eq. (13). The reference hologram is the previous partial digital hologram of  $U_D(x,y)$ , while the input hologram is obtained by placing a window with the same size centered at the origin of  $U_G(x,y)$ .

In Fig. 15 we show the correlation obtained by digital holography between the 3D object in Fig. 13(a) used as a reference, and the same slightly rotated 3D object used as input. We utilized a window centered at the origin of the reference hologram and the same window shifted to different positions in the input hologram. Figure 15(a) shows the maximum peak of the correlation as a function of the displacement of the window in the hologram of the input. A sharp intensity peak is obtained for an angle of view  $(\alpha,\beta)=(0.007^\circ,0.001^\circ)$ . Figure 15(b) shows the correlation for this perspective of the 3D object. From this results we can measure the orientation of the input respect to the reference object. Note that other processing operations can be easily applied to the 3D image.

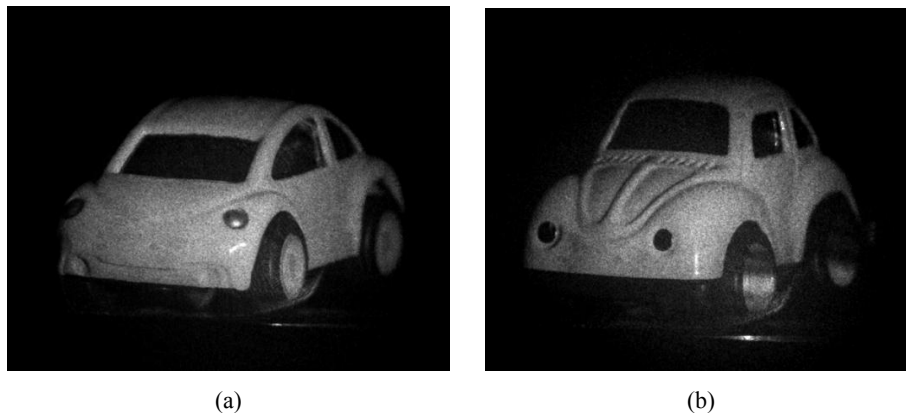


Figure 13. (a) Reference and (b) input 3D objects.

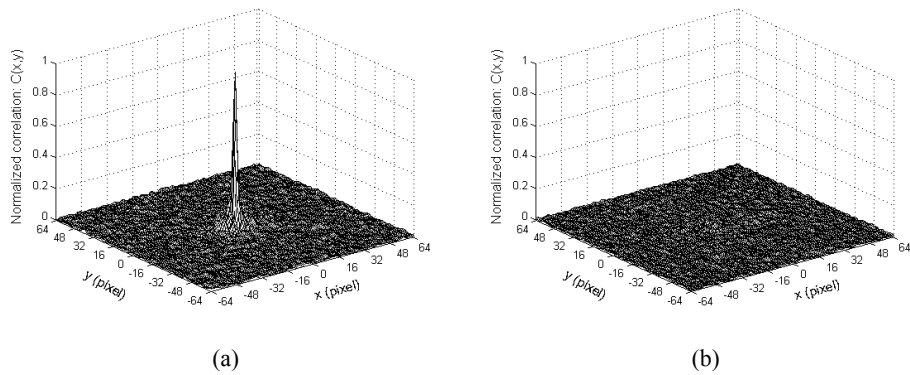


Figure 14. (a) Autocorrelation and (b) crosscorrelation of the 3D objects represented in Fig. 13 carried out by digital holography.

### 5. CONCLUSIONS

We have described several optoelectronic techniques based on digital phase-shifting holography for security applications. Information codified as both 2D and 3D images is optically processed and captured electronically. These techniques combine the high space-bandwidth product and speed of optical processing with the advantages of electronic transmission, storage, and post-processing.

Encryption of 2D images into a random complex pattern is performed using two random phase masks in a phase-shifting interferometer architecture. Electronic decryption can be achieved using a one-step FFT reconstruction procedure but only having the proper key. Alternatively, decryption can be performed optically by encoding the digital hologram as a computer generated one and displaying it on a spatial light modulator.

A similar technique has been described to encrypt information encoded as a 3D image. Once decrypted, the 3D input object can be reconstructed from different perspectives in the computer.

Also, we have explained a method to reconstruct optically a 3D object from its digital hologram. The reconstruction is performed by use of phase-only information. In this way, we are able to use commercially available displays to encode the digital hologram.

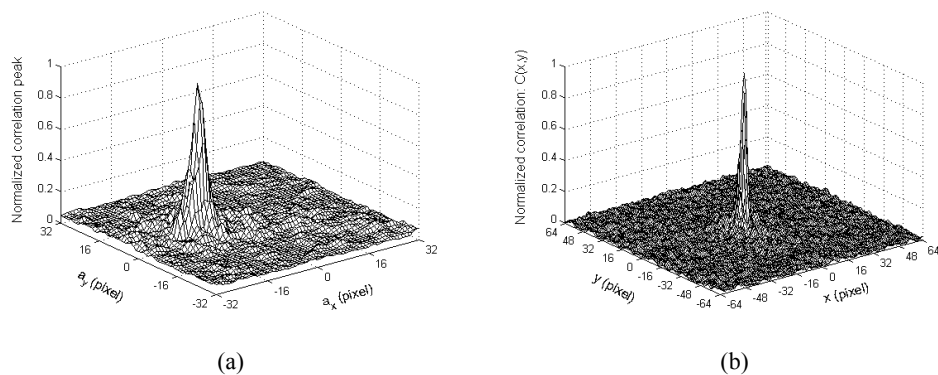


Figure 15. Correlation of the 3D object in Fig. 13 (a) with a rotated version of the same 3D object obtained by digital holography: (a) correlation peak versus the angle of view, and (b) correlation for the angle giving the maximum peak.

Finally, we have described a method to perform pattern recognition of 3D objects. The method allows us to obtain 3D information of the reference and input objects in a single step. Recognition is carried out by a digital matched filter technique applied to the holographic information. Furthermore, this technique can measure small orientation changes of the 3D object.

Other optoelectronic 3D image processing operations based in the above methods are also possible. As we will show in the presentation, we have extended the pattern recognition method to achieve shift invariance along the optical axis. Furthermore, we have used nonlinear composite correlation filters and a two-layer neural network for processing of 3D images that are obtained by digital holography. This allows us to achieve distortion tolerance. Moreover, we have applied compression techniques to digital holograms for the efficient transmission of 3D images.

## REFERENCES

1. H.-Y. Li, Y. Qiao, and D. Psaltis, "Optical network for real-time face recognition," *Appl. Opt.* **32**, 5026-5035 (1993).
2. B. Javidi and J. L. Horner, "Optical pattern recognition for validation and security verification," *Opt. Eng.* **33**, 1752-1756 (1994).
3. Ph. Réfrégier and B. Javidi, "Optical image encryption based on input plane and Fourier plane random encoding," *Opt. Lett.* **20**, 767-769 (1995).
4. C. L. Wilson, C. I. Watson, and E. G. Paek, "Combined optical and neural network fingerprint matching," *Proc. SPIE* **3073**, 373-382 (1997).
5. N. Yoshikawa, M. Itoh, and T. Yatagai, "Binary computer-generated holograms for security applications from a synthetic double-exposure method by electron-beam lithography," *Opt. Lett.* **23**, 1483-1485 (1998).
6. O. Matoba and B. Javidi, "Encrypted optical memory system using three-dimensional keys in the Fresnel domain," *Opt. Lett.* **24**, 762-764 (1999).
7. J. E. Ford, Y. Fainman, and S. H. Lee, "Array interconnection by phase-coded optical correlation," *Opt. Lett.* **15**, 1088-1090 (1990).
8. C. Denz, G. Pauliat, G. Roosen, and T. Tschudi, "Volume hologram multiplexing using a deterministic phase encoding method," *Opt. Commun.* **85**, 171-176 (1991).
9. H. Lee and S. K. Jin, "Experimental study of volume holographic interconnects using random patterns," *Appl. Phys. Lett.* **62**, 2191-2193 (1993).
10. J. F. Heanue, M. C. Bashaw, and L. Hesselink, "Encrypted holographic data storage based on orthogonal-phase-code multiplexing," *Appl. Opt.* **34**, 6012-6015 (1995).
11. C. Denz, K. O. Mueller, F. Visinka, and T. T. Tschudi, "Digital volume holographic data storage using phase-coded multiplexing," *Proc. SPIE* **3802**, 142-147 (1999).
12. C. C. Sun, W. C. Su, B. Wang, and Y. Ouyang, "Diffraction selectivity of holograms with random phase encoding," *Opt. Commun.* **175**, 67-74 (2000).
13. U. Schnars and W. P. O. Jüptner, "Direct recording of holograms by a CCD target and numerical reconstruction," *Appl. Opt.* **33**, 179-181 (1994).
14. Y. Takaki, H. Kawai, and H. Ohzu, "Hybrid holographic microscopy free of conjugate and zero-order images," *Appl. Opt.* **38**, 4990-4996 (1999).
15. E. Cucho, F. Bevilacqua, and C. Depeursinge, "Digital holography for quantitative phase-contrast imaging," *Opt. Lett.* **24**, 291-293 (1999).
16. J. H. Bruning, D. R. Herriott, J. E. Gallagher, D. P. Rosenfeld, A. D. White, and D. J. Brangaccio, "Digital wave-front measuring interferometer for testing optical surfaces and lenses," *Appl. Opt.* **13**, 2693-2703 (1974).
17. J. Schwider, "Advanced evaluation techniques in interferometry," in: *Progress in Optics*, Vol. XXVIII, ed. E. Wolf, pp. 271-359 (North-Holland, Amsterdam, 1990).
18. I. Yamaguchi and T. Zhang, "Phase-shifting digital holography," *Opt. Lett.* **22**, 1268-1270 (1997).
19. B. Javidi and T. Nomura, "Securing information by means of digital holography," *Opt. Lett.* **25**, 28-30 (2000).
20. E. Tajahuerce, O. Matoba, S.C. Verrall, and B. Javidi, "Optoelectronic information encryption with phase-shifting interferometry," *Appl. Opt.* **39**, 2313-2320 (2000).
21. E. Tajahuerce and B. Javidi, "Encrypting three-dimensional information with digital holography," *Appl. Opt.* **39**, 6595-6601 (2000).
22. O. Matoba, T.J. Naughton, Y. Frauel, N. Bertaux, and B. Javidi, "Real-time three-dimensional object reconstruction using phase-only digital hologram," *Appl. Opt.* **41**, 6187-6192 (2002).

23. B. Javidi and E. Tajahuerce, "Three dimensional object recognition using digital holography", *Opt. Lett.* **25**, 610-612 (2000).
24. E. Tajahuerce, O. Matoba, and B. Javidi, "Shift-invariant three-dimensional object recognition by means of digital holography", *Appl. Opt.* **40**, 3877-3886 (2001).
25. Y. Frauel, E. Tajahuerce, M.A. Castro, and B. Javidi, "Distortion-tolerant three-dimensional object recognition with digital holography", *Appl. Opt.* **40**, 3887-3893 (2001).
26. Y. Frauel and B. Javidi, "Neural network for three-dimensional object recognition based on digital holography", *Opt. Lett.* **26**, 1478-1480 (2001).
27. T.J. Naughton, Y. Frauel, B. Javidi, and E. Tajahuerce, "Compression of digital holograms for three-dimensional object reconstruction and recognition", *Appl. Opt.* **41**, 4124-4132 (2002).
28. T.J. Naughton, J.B. McDonald, and B. Javidi, "Efficient compression of Fresnel fields for internet transmission of three-dimensional images", *Appl. Opt.* **42**, 4758-4764 (2003).
29. Y. Frauel, E. Tajahuerce, O. Matoba, A. Castro, and B. Javidi, "Comparison of passive ranging integral imaging and active imaging digital holography for three-dimensional object recognition", *Appl. Opt.* **43**, 452-462 (2004).
30. J.W. Cooley, J. W. Tukey, "An algorithm for the machine calculation of complex Fourier series" *Math. Comput.* **19**, 297-301 (1965).